International Journal of Heat and Mass Transfer 52 (2009) 1853–1863

Contents lists available at ScienceDirect

International Journal of Heat and Mass Transfer

journal homepage: www.elsevier.com/locate/ijhmt

Experimental study of saturated flow boiling heat transfer in an array of staggered micro-pin-fins

Weilin Qu *, Abel Siu-Ho

Department of Mechanical Engineering, University of Hawaii at Manoa, Honolulu, HI 96822, USA

ARTICLE INFO

Article history:
Received 28 May 2008
Available online 4 December 2008

Keywords:
Micro-pin-fin array
Saturated flow boiling
Heat transfer
Micro-scale enhancement structure

ABSTRACT

This study concerns water saturated flow boiling heat transfer in an array of staggered square micro-pin-fins having a $200 \times 200\ \mu m^2$ cross-section by a 670 μm height. Three inlet temperatures of 90, 60, and 30 °C, six mass velocities for each inlet temperature, ranging from 183 to 420 kg/m^2 s, and outlet pressures between 1.03 and 1.08 bar were tested. Heat fluxes ranged from 23.7 to 248.5 W/cm^2. Heat transfer coefficient was fairly constant at high quality, insensitive to both quality and mass velocity. Heat transfer was enhanced by inlet subcooling at low quality. Possible heat transfer mechanism was discussed.

1. Introduction

Two-phase miniature heat sinks that incorporate micro-scale internal heat transfer enhancement structures that are tens to hundreds of micrometers in size and capitalize on latent heat exchange through liquid flow boiling have recently emerged as a highly efficient cooling technique to meet the current and future high heat flux dissipation needs in many cutting-edge technologies. Key technical merits of these heat sinks include very high heat transfer coefficient, small overall heat sink mass and size, small liquid coolant storage and flow rate requirements, and uniform temperature distribution in the stream-wise direction. Among a wide variety of possible micro-scale enhancement structures, parallel micro-channels have received the most attention (Fig. 1(a)). Flow boiling heat transfer in micro-channels has been studied quite extensively in the past decade with the aim to establish reliable predictive tools for effective heat sink design [1–8]. Results from these studies indicated that the micro-scale channel size had a profound effect on liquid flow boiling behavior, and heat transfer correlations developed for conventional size channels were unable to predict micro-channel flow boiling data.

Recent advancement in micro-fabrication techniques, however, allows more complex micro-scale geometries to be fabricated into high-thermal-conductivity solid substrate at low cost, which makes it possible to explore other enhancement structures that may be more effective than the aforementioned parallel micro-channels. A promising configuration is arrays of staggered or aligned micro-size pin-fins (Fig. 1(b) and (c)) [9–17]. Performance assessment of micro-pin-fin arrays as alternative enhancement structures for two-phase miniature heat sinks requires a fundamental understanding and accurate prediction of flow boiling heat transfer in the configuration. Although there are a number of studies on single-phase convective heat transfer in micro-pin-fin arrays [9–15], studies on flow boiling heat transfer are rather scarce [16,17].

Koşar and Peles investigated flow boiling heat transfer of refrigerant R-123 in an array of hydrofoil pin-fins with chord thickness of 100 μm and height H_{fin} of 243 μm [16]. They found that at low quality heat transfer coefficient increased with increasing heat flux, which might be attributed to the nucleate boiling heat transfer mechanism. At high quality, heat transfer coefficient decreased with increasing heat flux, which might be linked to convective boiling heat transfer mechanism. Flow patterns were identified to be bubbly, wavy intermittent, and spray-annular depending on heat flux and mass velocity. Previous heat transfer correlations developed for conventional size tube bundles could not predict their experimental data. Two new heat transfer correlations were proposed.

Krishnamurthy and Peles experimentally studied water flow boiling heat transfer in an array of staggered circular pin-fins with diameter d of 100 μm, height to diameter ratio H_{fin}/d of 2.5, longitudinal pitch to diameter ratio S_L/d of 1.5, and transverse pitch to diameter ratio S_T/d of 1.5 [17]. They found that heat transfer coefficient was moderately dependent on mass flux and independent of heat flux. Flow patterns were identified to be vapor slug and annular flow. Based on the observed dominant annular flow pattern and characteristics of heat transfer coefficient, the heat transfer mechanism was determined to be convective boiling. Two new heat transfer correlations based on the convective boiling mechanism

* Corresponding author. Tel.: +1 808 956 6332; fax: +1 808 956 2373.
E-mail address: qu@hawaii.edu (W. Qu).

0017-9310/$ - see front matter © 2008 Elsevier Ltd. All rights reserved.
doi:10.1016/j.ijheatmasstransfer.2008.10.008

Nomenclature

a_0, a_1, a_2	empirical constants in present correlation
A_c	cross-sectional area of a micro-pin-fin
A_{cell}	unit cell base area
A_{fin}	wetted surface area of a micro-pin-fin
A_{min}	minimum transverse flow area of micro-pin-fin array
A_t	platform area of heat sink top surface
$c_{p,f}$	specific heat of liquid water
d	diameter of circular pin-fin
d_e	equivalent diameter of a square micro-pin-fin
$f_{fin,sub,i}$	friction factor in segment i
F	subcooling enhancement factor in present correlation
G	mass velocity
G_{max}	maximum mass velocity
h_{tp}	saturated flow boiling heat transfer coefficient
$h_{tp,eq}$	saturated flow boiling heat transfer coefficient in high x_e region for a near saturated inlet
$h_{tp,tci}$	saturated flow boiling heat transfer coefficient at thermocouple stream-wise location
H_{fin}	height of a pin-fin
H_{tc}	distance from thermocouple to micro-pin-fin base
i	a stream-wise segment containing one row of micro-pin-fins
k	thermal conductivity
K_{c1}, K_{c2}	contraction loss coefficient
K_{e1}, K_{e2}	expansion recovery coefficient
L	length of heat sink top platform area
L_{fin}	length of a micro-pin-fin
$\dot{m}$	total mass flow rate
m_{fin}	fin parameter
M	number of data points
MAE	mean absolute error
N_{sub}	number of micro-pin-fin rows in upstream subcooled region
P_{fin}	cross-section perimeter of a micro-pin-fin
$P_{fin,in}$	micro-pin-fin array inlet pressure
$P_{fin,out}$	micro-pin-fin array outlet pressure
P_{in}	measured heat sink inlet pressure
P_{out}	heat sink outlet pressure
$P_{sat,0}$	pressure at $z_{sat,0}$
P_{tci}	pressure at thermocouple stream-wise location
P_W	total electrical power input
ΔP	measured pressure drop across heat sink
ΔP_{c1}, ΔP_{c2}	contraction pressure loss
ΔP_{e1}, ΔP_{e2}	expansion pressure recovery
ΔP_{fin}	pressure drop across micro-pin-fin array
Pr	Prandtl number
q''_{eff}	heat flux based on heat sink top platform area
Q_{loss}	heat loss
S_D	diagonal pitch
S_L	longitudinal pitch
S_T	transverse pitch
Re	Reynolds number based on d_e
Re_f	Reynolds number based on d_e and actual liquid flow rate
tci	thermocouple (i = 1–3)
T	temperature
$T_{f,tci}$	water bulk temperature at thermocouple stream-wise location
T_{in}	inlet temperature
T	outlet temperature
$T_{sat,0}$	saturation temperature at $z_{sat,0}$
$T_{sat,in}$	saturation temperature at micro-pin-fin array inlet
$T_{sat,tci}$	saturation temperature at thermocouple stream-wise location
T_{tci}	thermocouple reading (i = 1–3)
$T_{w,tci}$	micro-pin-fin base temperature at thermocouple stream-wise location
v	specific volume
v_{fg}	specific volume difference between saturated vapor and saturated liquid
W	width of heat sink top platform area
W_{fin}	width of a micro-pin-fin
x_e	thermodynamic equilibrium quality
$x_{e,tci}$	thermodynamic equilibrium quality at thermocouple stream-wise location
X_{vv}	Martinelli parameter
z	steam-wise coordinate
$z_{sat,0}$	stream-wise location where thermodynamic equilibrium quality is zero
z_{tci}	steam-wise location of thermocouple (i = 1–3)

Greek symbols

φ_l	two-phase frictional multiplier
η_{fin}	fin efficiency
μ	viscosity
ζ	adjustment parameter in the Krishnamurthy and Peles correlations (correlations 1 and 2)

Subscripts

ave	average
exp	experimental (measured)
f	liquid (water) bulk
g	vapor
i	stream-wise segment
in	inlet
out	outlet
$pred$	predicted
$p1$	deep plenum
$p2$	shallow plenum
s	solid (copper)
sub	upstream subcooled region
tci	thermocouple stream-wise location (i = 1–3)

and Reynolds analogy were proposed, which showed reasonable agreement with their experimental data.

Other relevant studies include those on flow boiling heat transfer in conventional size tube bundles that are several millimeters or larger in diameter [18–23]. Tube bundles are widely used in two-phase heat exchanger applications such as chemical reboilers, steam generators, and evaporators. Although both involve boiling heat transfer associated with liquid cross flow, results from these tube bundles studies should not be directly applied to micro-pin-fin arrays because of the following two factors: (a) diminishing flow passage size may affect flow boiling heat transfer characteristics substantially as demonstrated by the aforementioned microchannel flow boiling studies [1–8], and (b) nearly all previous tube bundle studies adopted aligned or in-line configuration while staggered arrangement was favored with micro-pin-fin heat sinks in order to achieve better heat transfer performance [16,17]. Deviation of flow boiling heat transfer characteristics in micro-pin-fin arrays from those in conventional size tube bundles has been discussed in the previous study by Koşar and Peles [16].

Despite the previous efforts [16,17], our fundamental knowledge of flow boiling heat transfer in micro-pin-fin arrays is far from complete. In particular, many unique parameter trends observed in

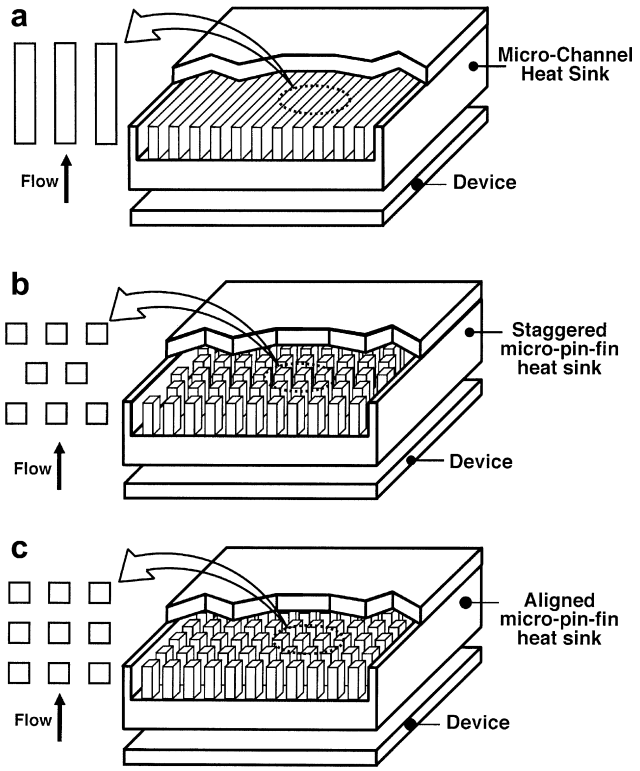

Fig. 1. (a) Micro-channel heat sink, (b) staggered micro-pin-fin heat sink, and (c) aligned micro-pin-fin heat sink.

micro-pin-fin arrays are not well understood, i.e., it is not clear what underlying transport process caused decreasing [16] or constant [17] heat transfer coefficient with increasing heat flux. In addition, a few proposed micro-pin-fin correlations have not been assessed using a sufficiently large database. This study expands on the previous studies by investigating water saturated flow boiling heat transfer in an array of staggered square micro-pin-fins with a cross-section of 200 × 200 μm^2 and a height of 670 μm. The objectives of the present study are: (1) to provide new heat transfer data for water flow boiling in a micro-pin-fin array, (2) to reveal important parametric trends and explore possible heat transfer mechanism, (3) to assess the accuracy of previous micro-pin-fin correlations at predicting the new data, and (4) to develop a new heat transfer correlation for water saturated flow boiling in the micro-pin-fin array.

2. Experimental apparatus and procedure

2.1. Flow loop

Fig. 2 shows a schematic of the flow loop that supplied the liquid coolant, deionized water, to a micro-pin-fin test module at desired operating conditions. Water was stored in a reservoir that also served as a pressure reference point for the flow loop. An immersion heater was installed in the reservoir to deaerate water through vigorous boiling to force any dissolved gases to escape to the ambient. The water was circulated using a gear pump. A compact heat exchanger connected to the laboratory tap water supply was used to bring the testing water to a temperature of approximately 19 °C before it entered the pump. After leaving the pump, the water flowed through a filter to prevent solid particles from clogging micro-size flow passages across the micro-pin-fin array. The water then passed through one of two rotameters for mass flow rate measurement. The rotameters were calibrated using the

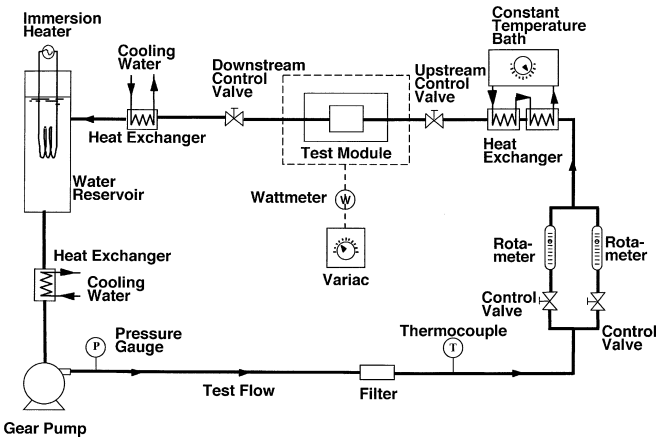

Fig. 2. Schematic of flow loop.

standard weighting method. The accuracy of mass flow rate measurement was better than 4% of the readings. Afterwards, the water flowed through a second heat exchanger that was connected to a constant temperature bath, where the water was brought to the desired test module inlet temperature. The water then entered the micro-pin-fin test module. The water exiting the test module flowed through a third heat exchanger that was also connected to the laboratory tap water supply to condense vapor before it returned to the reservoir.

2.2. Test module

The test module was composed of a 110 copper micro-pin-fin heat sink, a G-7 fiberglass plastic housing, a polycarbonate plastic (Lexan) cover plate, and nine cartridge heaters. Fig. 3 illustrates all test module components. The micro-pin-fin heat sink had a platform (top) area of 3.38 cm (length) by 1.0 cm (width). An array of 1950 staggered micro-pin-fins with a 200 × 200 μm^2 cross-section by a 670 μm height were milled out of the top surface using a micro-end mill. Dimensions of the micro-pin-fins were measured using a scanning electron microscope (SEM). Uncertainty in W_{fin} and L_{fin} was estimated to be ±5 μm, and in H_{fin} was ±10 μm. SEM Images showed the surface roughness of the micro-pin-fins was in the order of 1 μm. Fig. 4(a) shows a top view of the micro-pin-fin array together with key dimensions. For the present micro-pin-fin array configuration, the ratio of the overall heat transfer area to the heat sink top platform area is equal to 3.9. Below the heat sink top surface, three Type-K thermocouples, indicated in Fig. 3 as *tc*1 to *tc*3 from upstream to downstream, were inserted along the center plane to measure the stream-wise temperature distribution inside the heat sink. The stream-wise distance of the three thermocouples from the micro-pin-fin array inlet, z_{tc1}, z_{tc3}, and z_{tc3}, is 5, 16.6, and 28.2 mm, respectively. Nine holes were drilled into the bottom surface of the heat sink to accommodate the cartridge heaters that provided heating power during the tests. The nine cartridge heaters were connected in parallel and powered by a 0–110 V AC variac. A 0.5% accuracy wattmeter was used to measure the total electrical power input to the cartridge heaters P_W.

The micro-pin-fin heat sink was inserted into the center portion of the G-7 housing with RTV silicone rubber applied along the interface to prevent leakage. Upstream and downstream of the micro-pin-fin array were plenums to ensure an even distribution of water flow across the micro-pin-fin array in the transverse direction. Each plenum had a deep portion leading to a shallow portion. Two Type-K thermocouples were located in the inlet and outlet deep plenums to measure the inlet and outlet temperature,

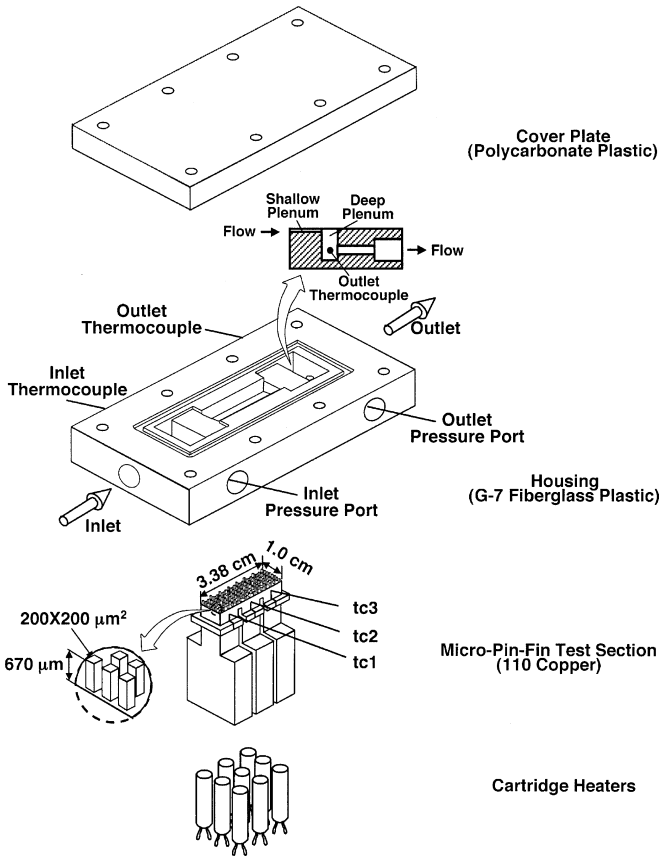

Fig. 3. Test module construction.

respectively. Errors associated with the measurements of these as well as the thermocouples inside the heat sink were smaller than ±0.3 °C. An absolute pressure transducer was connected to the inlet deep plenum via a pressure tap to measure the heat sink inlet pressure. A differential pressure transducer was connected to the inlet and outlet deep plenums to measure the pressure drop across the heat sink. The uncertainty in both inlet pressure and pressure drop measurements was estimated to be less than 0.25% of the readings. The readings of pressure transducers and thermocouples were recorded using an PC based data acquisition system.

Closed flow passages across the micro-pin-fin array were formed by bolting the cover plate atop the heat sink and housing. A shallow groove was machined into the housing around the heat sink top surface. The groove was filled with RTV silicone rubber to create a leak-proof seal. The transparent cover plate allowed direct visual access to liquid–vapor two-phase flow in the micro-pin-fin array.

After the test module was assembled, multiple layers of ceramic fiber were wrapped around the heat sink to reduce the heat loss to the ambient.

2.3. Experimental procedure

Prior to conducting a flow boiling test, the water in the reservoir was deaerated through vigorous boiling for about an hour to force any dissolving gases to escape to the ambient. Effectiveness of this deaeration method was verified by visually observing the gas bubble activity in the micro-pin-fin array during the flow boiling test. It was observed that no gas/air bubble coming out of the water inside the micro-pin-fin array prior to boiling incipience. At boiling incipience, the reading from the downstream thermocouple *tc*3, which was the highest among those from the thermocouples *tc*1 to *tc*3, was above 100 °C, and nucleation of water vapor bubbles occurred inside the micro-pin-fin array. The flow loop components were then adjusted to yield the desired test module inlet temperature T_{in} and mass flow rate $\dot{m}$. Table 1 summarizes the operating conditions in the present study. G_{max} in Table 1 indicates the maximum water mass velocity in the micro-pin-fin array and is defined based on the minimum transverse flow area,

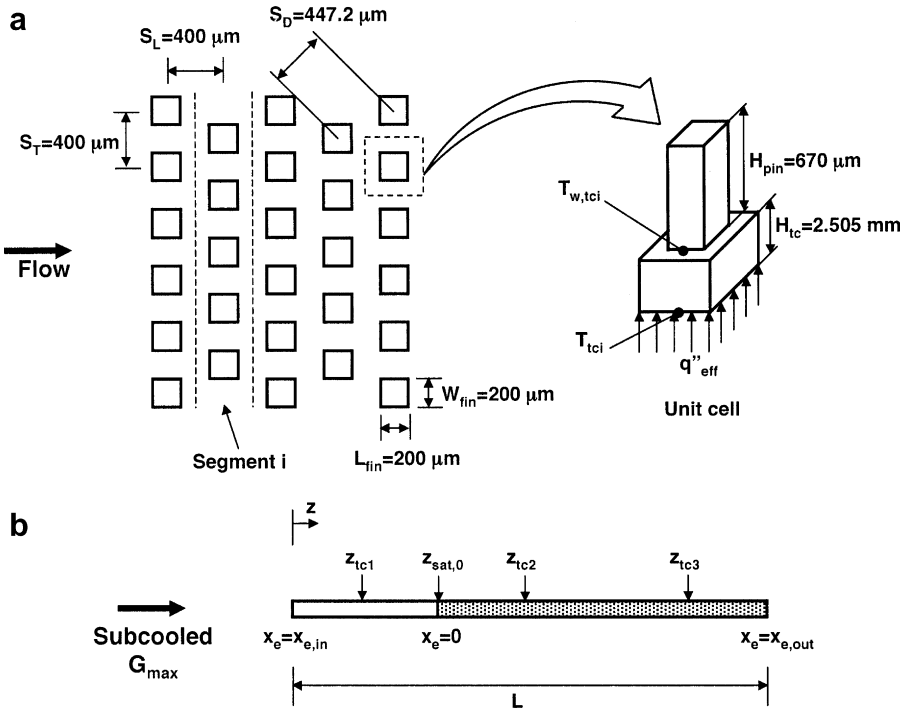

Fig. 4. (a) Top view of micro-pin-fin array and schematic of unit cell. (b) Schematic of flow regions.

Table 1
Operating conditions.

Inlet temperature, T_{in} (°C)	Mass flow rate, $\dot{m}$ (g/s)	Maximum mass velocity, G_{max} (kg/m^2 s)	Outlet pressure, P_{out} (bar)
90	0.611–1.398	183–417	1.03–1.08
60	0.611–1.398	183–417	1.03–1.08
30	0.611–1.408	183–420	1.03–1.08

$$G_{max} = \frac{\dot{m}}{A_{min}}, \tag{1}$$

where

$$A_{min} = WH_{fin}\left(1 - \frac{W_{fin}}{S_T}\right). \tag{2}$$

P_{out} represents the heat sink outlet pressure and is evaluated from the measured heat sink inlet pressure P_{in} and pressure drop ΔP.

$$P_{out} = P_{in} - \Delta P. \tag{3}$$

As shown in Table 1, the flow boiling tests were performed at near-ambient pressures with P_{out} ranging from 1.03 to 1.08 bar.

After the flow became stable, the heating power was set to a low level where the water flow in the micro-pin-fin array remained single-phase liquid. The power was then increased in small increments as the flow loop components were adjusted to maintain the desired inlet temperature and mass flow rate as given in Table 1. At each new heating power level, the heat sink was allowed to reach steady state conditions. Once at steady state, readings from the pressure transducers and thermocouples were recorded at 0.5-s intervals for 3 min using the data acquisition system. Readings from the rotameter and wattmeter were recorded manually.

Prior to conducting flow boiling experiments, a series of water single-phase heat transfer tests were conducted at the same mass flow rates. Results from these single-phase tests were reported in a separate paper [15]. During single-phase tests, heat losses from the test module were evaluated by deducting the measured enthalpy increase of the water flow from the total electrical power input measured by the wattmeter.

$$Q_{loss} = P_W - \dot{m}c_{p,f}(T_{out} - T_{in}). \tag{4}$$

For T_{in} = 30 °C, Q_{loss} ranged from 3% to 15% of P_W [15]. Higher heat losses occurred at lower water mass flow rates. For a given water mass flow rate, it has been observed that Q_{loss} was not sensitive to the electrical power input.

In the present study, the level of input heat flux that was removed by the water flow boiling from the micro-pin-fin array is represented by an effective heat flux q''_{eff}, defined based on the top platform area of the heat sink, A_t = 1.0 × 3.38 cm^2.

$$q''_{eff} = \frac{P_W - Q_{loss,ave}}{A_t}, \tag{5}$$

where $Q_{loss,ave}$ is the average heat loss obtained from the single-phase tests at the same mass flow rate.

Each test was terminated when the reading from the downstream thermocouple *tc*3 inside the heat sink reached about 130 °C to avoid overheating the test module.

2.4. Data reduction

In the present study, the water was supplied to the micro-pin-fin array in a subcooled state ($T_{in} < T_{sat,in}$) for all operating conditions as shown in Table 1. The micro-pin-fin array can therefore be divided into two regions along the stream-wise direction based on the value of water thermodynamic equilibrium quality x_e: an upstream subcooled region ($x_e < 0$) and a downstream saturated boiling region ($x_e \geqslant 0$). Fig. 4(b) shows a schematic of the two flow regions. The stream-wise location $z_{sat,0}$ where x_e reached zero serves as a dividing point between the two regions. $z_{sat,0}$ is evaluated from

$$Z_{sat,0} = \frac{\dot{m}c_{p,f}(T_{sat,0} - T_{in})}{q''_{eff}W}, \tag{6}$$

where $T_{sat,0}$ is the saturation temperature at $z_{sat,0}$ corresponding to local pressure $P_{sat,0}$. The following equation is employed to evaluate $P_{sat,0}$:

$$P_{sat,0} = P_{fin,in} - \Delta P_{fin,sub}, \tag{7}$$

where $P_{fin,in}$ is the pressure at the micro-pin-fin array inlet, and $\Delta P_{fin,sub}$ is the pressure drop across the upstream subcooled region $0 \leqslant z \leqslant z_{sat,0}$. $P_{fin,in}$ is evaluated by deducting inlet contraction pressure losses from the measured heat sink inlet pressure P_{in},

$$P_{fin,in} = P_{in} - (\Delta P_{c1} + \Delta P_{c2}). \tag{8}$$

ΔP_{c1} and ΔP_{c2} in Eq. (8) are the contraction pressure losses from the housing deep plenum to the shallow plenum and from the shallow plenum to the micro-pin-fin array, respectively, and are calculated from [24,25]

$$\Delta P_{c1} = \frac{v_{f,in}}{2}(G^2_{p2,in} - G^2_{p1,in}) + \frac{K_{c1}v_{f,in}}{2}G^2_{p2,in}, \tag{9}$$

and

$$\Delta P_{c2} = \frac{v_{f,in}}{2}(G^2_{max} - G^2_{p2,in}) + \frac{K_{c2}v_{f,in}}{2}G^2_{max}. \tag{10}$$

$\Delta P_{fin,sub}$ is determined using the following pressure drop correlation developed by the present authors for water single-phase flow in the micro-pin-fin array [24].

$$\Delta P_{fin,sub} = \sum_{i=1}^{N_{sub}} \Delta P_{fin,sub,i} = \sum_{i=1}^{N_{sub}} \left[f_{fin,sub,i}\left(\frac{\mu_{f,i}}{\mu_{w,i}}\right)^{0.58} \frac{v_{f,i}G^2_{max}}{2} \right], \tag{11}$$

where N_{sub} is the number of micro-pin-fin rows in the subcooled region, i indicates a segment in the stream-wise direction that contains a row of micro-pin-fins as well as the surrounding portion of the top and bottom endwalls as shown in Fig. 4(a), and $f_{fin,sub,i}$ represents the friction factor across the segment i and is determined from [24]

$$f_{fin,sub,i} = 20.09Re^{-0.547}_{fin,sub,i} = 20.09\frac{G_{max}d_e}{\mu_{f,i}}^{-0.547}. \tag{12}$$

d_e in Eq. (12) represents an equivalent diameter of the square micro-pin-fins,

$$d_e = \frac{4A_c}{P_{fin}}, \tag{13}$$

where A_c is the cross-sectional area of a single micro-pin-fin,

$$A_c = W_{fin}L_{fin}, \tag{14}$$

and P_{fin} is the cross-section perimeter of a single micro-pin-fin,

$$P_{fin} = 2(W_{fin} + L_{fin}). \tag{15}$$

All water properties in Eq. (11) except $\mu_{w,i}$ are evaluated based on the average water bulk temperature in the segment i. $\mu_{w,i}$ is evaluated based on the average micro-pin-fin base temperature in the segment i. For brevity, details on how to evaluate these properties are omitted from this paper and can be found in Ref. [24].

Once $z_{sat,0}$ is obtain from Eq. (6), it is easy to determine whether each thermocouple stream-wise location z_{tci} is within the upstream subcooled region $0 \leqslant z_{tci} \leqslant z_{sat,0}$ or the downstream saturated boiling region $z_{sat,0} \leqslant z_{tci} \leqslant L$. For $z_{sat,0} \leqslant z_{tci} \leqslant L$, the local

saturated flow boiling heat transfer coefficient averaged over the four surfaces (upstream, downstream, and side) of a single micro-pin-fin as well as the surrounding portion of the base surface at z_{tci}, $h_{tp,tci}$, can be evaluated by using the following equation:

$$q''_{eff}A_{cell} = h_{tp,tci}(T_{w,tci} - T_{sat,tci})[(A_{cell} - A_c) + \eta_{fin}A_{fin}]. \quad (16)$$

Eq. (16) is obtained by applying a simple energy balance to a unit cell at z_{tci} that contains a single micro-pin-fin as well as the surrounding base surface as shown in Fig. 4(a). The left-hand side of Eq. (16) represents the heat input to the unit cell, and the right-hand side the heat removal from the unit cell by the water flow boiling. In Eq. (16), A_{cell} indicates the unit cell base area,

$$A_{cell} = S_L S_T, \quad (17)$$

A_{fin} is the wetted surface area of a single pin-fin,

$$A_{fin} = P_{fin}H_{fin}, \quad (18)$$

and η_{fin} represents the fin efficiency,

$$\eta_{fin} = \frac{tanh(m_{fin}H_{fin})}{m_{fin}H_{fin}}, \quad (19)$$

where m_{fin} is the fin parameter,

$$m_{fin} = \sqrt{\frac{h_{tp,tci}P_{fin}}{k_s A_c}}. \quad (20)$$

$T_{w,tci}$ and $T_{sat,tci}$ in Eq. (16) represent the local micro-pin-fin base temperature and the local water saturation temperature, respectively. Assuming one-dimensional heat conduction between the thermocouple location and the micro-pin-fin base as shown in Fig. 4(a), $T_{w,tci}$ is evaluated from

$$T_{w,tci} = T_{tci} - \frac{q''_{eff}H_{tc}}{k_s}, \quad (21)$$

where T_{tci} represents the readings from the thermocouple *tci*. $T_{sat,tci}$ is evaluated from the local pressure P_{tci}. Assuming a linear decrease in local pressure in the saturated boiling region $z_{sat,0} \leqslant z_{tci} \leqslant L$, P_{tci} is calculated from

$$P_{tci} = P_{sat,0} - \frac{P_{sat,0} - P_{fin,out}}{L - z_{sat,0}}(z_{tci} - z_{sat,0}), \quad (22)$$

where $P_{fin,out}$ represents the pressure at the micro-pin-fin array outlet and is evaluated by adding the outlet expansion pressure recoveries to the heat sink outlet pressure P_{out}.

$$P_{fin,out} = P_{out} + (\Delta P_{e2} + \Delta P_{e1}). \quad (23)$$

ΔP_{e2} and ΔP_{e1} in Eq. (23) are expansion pressure recoveries from the micro-pin-fin array to the housing shallow plenum and from the shallow plenum to the deep plenum, respectively, and are calculated from [24–26]

$$\Delta P_{e2} = \frac{v_{f,out} + x_{e,out}v_{fg,out}}{2}(G^2_{p2,out} - G^2_{max}) + \frac{K_{e2}(v_{f,out} + x_{e,out}v_{fg,out})}{2}G^2_{max}, \quad (24)$$

and

$$\Delta P_{e1} = \frac{v_{f,out} + x_{e,out}v_{fg,out}}{2}(G^2_{p1,out} - G^2_{p2,out}) + \frac{K_{e1}(v_{f,out} + x_{e,out}v_{fg,out})}{2}G^2_{p2,out}. \quad (25)$$

Once $T_{w,tci}$ and $T_{sat,tci}$ are determined, the value of $h_{tp,tci}$ can be readily calculated from Eq. (16). Eq. (16) is a transcendental equation, which can be solved iteratively to obtain $h_{tp,tci}$. For the present operating conditions as shown in Table 1, z_{tc1} was always in the subcooled region, i.e., $z_{tc1} < z_{sat,0}$. $h_{tp,tci}$ values were therefore obtained only at z_{tc2} and z_{tc3}. Only $h_{tp,tci}$ values corresponding to $x_{e,tci} \geqslant 0.01$ are reported in this paper to ensure that the saturated flow boiling conditions were well established. The uncertainty in $h_{tp,tci}$ is calculated using the method developed by Kline and McClintock [27]. The uncertainty ranges from 3.1% to 34.5%, with an average of 8.3%. The best uncertainty in $h_{tp,tci}$ occurs at z_{tc3} under the condition of T_{in} = 30 °C, G_{max} = 183 kg/m^2 s, q''_{eff} = 198.5 W/cm^2, and $x_{e,tc3}$ = 0.27. The worst uncertainty in $h_{tp,tci}$ occurs also at z_{tc3} under the condition of T_{in} = 90 °C, G_{max} = 228 kg/m^2 s, q''_{eff} = 48.0 W/cm^2, and $x_{e,tc3}$ = 0.05.

3. Results and discussion

3.1. Boiling curve

Fig. 5 shows boiling curves obtained at z_{tc1} to z_{tc3} for T_{in} = 60 °C and G_{max} = 260 kg/m^2 s. In these curves, q''_{eff} is plotted versus the difference between $T_{w,tci}$ and $T_{f,tci}$, where $T_{f,tci}$ represents the local water bulk temperature. For $0 \leqslant z_{tci} \leqslant z_{sat,0}$, $T_{f,tci}$ is evaluated from the following equation by assuming a linear increase in water temperature along the flow direction:

$$T_{f,tci} = T_{in} + (T_{sat,0} - T_{in})\frac{z_{tci}}{z_{sat,0}}. \quad (26)$$

For $z_{sat,0} \leqslant z_{tci} \leqslant L$,

$$T_{f,tci} = T_{sat,tci}. \quad (27)$$

Three regions featuring drastically different relationships between q''_{eff} and $(T_{w,tci} - T_{f,tci})$ can be readily identified at z_{tc2} and z_{tc3}: a low q''_{eff} single-phase region where the slopes of the boiling curves are positive and fairly constant, an intermediate q''_{eff} subcooled flow boiling region where the slopes of the boiling curves become negative due to a sharp rise in the convective heat transfer coefficient, and a high q''_{eff} saturated flow boiling region where the local thermodynamic equilibrium quality $x_{e,tci}$ is above zero and the slopes of the boiling curves are again positive. Transition from one region to another occurs at a lower q''_{eff} value at z_{tc3} than that at z_{tc2}, indicating that the boiling front propagated from downstream to upstream. z_{tc1} is always in the single-phase region.

3.2. Heat transfer characteristics

Figs. 6–8 plot all $h_{tp,tci}$ data obtained in this study for T_{in} = 90, 60, and 30 °C, respectively. Each figure consists of two parts: part (a)

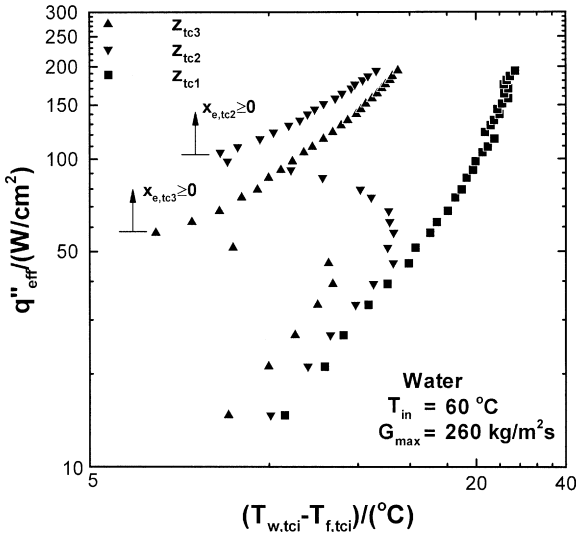

Fig. 5. Boiling curves at z_{tc1} to z_{tc3} for T_{in} = 60 °C and G_{max} = 260 kg/m^2 s.

plots $h_{tp,tci}$ versus $x_{e,tci}$, and part (b) $h_{tp,tci}$ versus q''_{eff}. The hollow symbols in Figs. 6–8 represent data points obtained at z_{tc2}, and the solid ones at z_{tc3}.

A close examination of part (a) of Figs. 6–8 reveals several important parametric trends. Firstly, for the highest T_{in} of 90 °C, Fig. 6(a) shows that $h_{tp,tci}$ is a weak function of $x_{e,tci}$ and tends to assume a constant value except in the very low $x_{e,tci}$ range. As T_{in} decreases from 90 to 60 °C and further to 30 °C, the dependence of $h_{tp,tci}$ on $x_{e,tci}$ becomes progressively stronger. For a constant G_{max}, Figs. 6(a)–8(a) show that $h_{tp,tci}$ decreases with increasing $x_{e,tci}$. $h_{tp,tci}$ decreases more rapidly at lower $x_{e,tci}$ and levels off at higher $x_{e,tci}$. Secondly, an increase in G_{max} from 183 to 420 kg/m^2 s at each T_{in} does not have an appreciable effect on $h_{tp,tci}$. For a fixed $x_{e,tci}$, $h_{tp,tci}$ is not very sensitive to G_{max}. Thirdly, for a given $x_{e,tci}$, $h_{tp,tci}$ does not show strong dependence upon the stream-wise location z_{tci}.

Part (b) of Figs. 6–8 illustrates the effect of q''_{eff} on $h_{tp,tci}$. For T_{in} = 90 °C, Fig. 6(b) shows that $h_{tp,tci}$ tends to assume a constant value except in the low q''_{eff} range for each G_{max}. For lower T_{in} of 60 and 30 °C, Figs. 7(b) and 8(b) show that for a constant G_{max}, $h_{tp,tci}$ decreases with increasing at low q''_{eff} and levels off at high q''_{eff}, and for a fixed q''_{eff}, $h_{tp,tci}$ increases with increasing G_{max}. In addition, for given q''_{eff} and G_{max}, $h_{tp,tci}$ at the upstream z_{tc2} has a higher value than that at the downstream z_{tc3}. These trends are consistent with

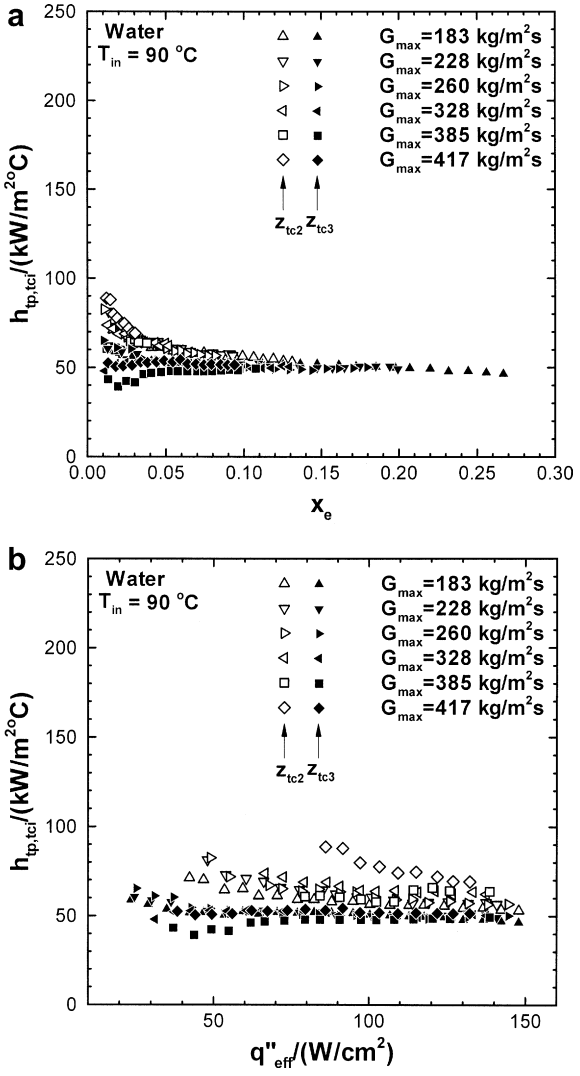

Fig. 7. Variation of measured $h_{tp,tci}$ with (a) $x_{e,tci}$ and (b) q''_{eff} for T_{in} = 60 °C.

those of constant $h_{tp,tci}$ for high T_{in} and decreasing $h_{tp,tci}$ with increasing $x_{e,tci}$ for low T_{in} as shown in Figs. 6(a)–8(a).

Figs. 6(a)–8(a) reveal that T_{in} has a considerable effect on the variation of $h_{tp,tci}$ with $x_{e,tci}$. To further illustrate the effect, $h_{tp,tci}$ versus $x_{e,tci}$ at z_{tc3} for three T_{in} and six G_{max} is plotted in a single graph, Fig. 9. It can be seen from Fig. 9 that for a given $x_{e,tc3}$, $h_{tp,tc3}$ increases with decreasing T_{in}, but is not sensitive to G_{max}. The trend implies that heat transfer in the saturated flow boiling region was enhanced by the inlet subcooling. The enhancement effect is more profound at low $x_{e,tc3}$, and diminishes as $x_{e,tc3}$ increases to a higher value.

Previous studies indicated that the two mechanisms of nucleate boiling and two-phase forced convection that govern saturated flow boiling heat transfer in conventional size tubes could also be applied to explain the observed parametric trends in tube bundles [18,19,22,23]. The regime dominated by nucleate boiling is usually associated with bubbly and slug flow. In this regime, liquid near the heated surface is superheated to a sufficient degree to sustain nucleation. Heat transfer coefficient is dependent upon heat flux, but fairly independent of mass velocity and vapor quality. The general trend is increasing heat transfer coefficient with increasing heat flux due to intensification of nucleation. The regime dominated by two-phase forced convection, on the other hand, is often associated with annular flow.

Fig. 6. Variation of measured $h_{tp,tci}$ with (a) $x_{e,tci}$ and (b) q''_{eff} for T_{in} = 90 °C.

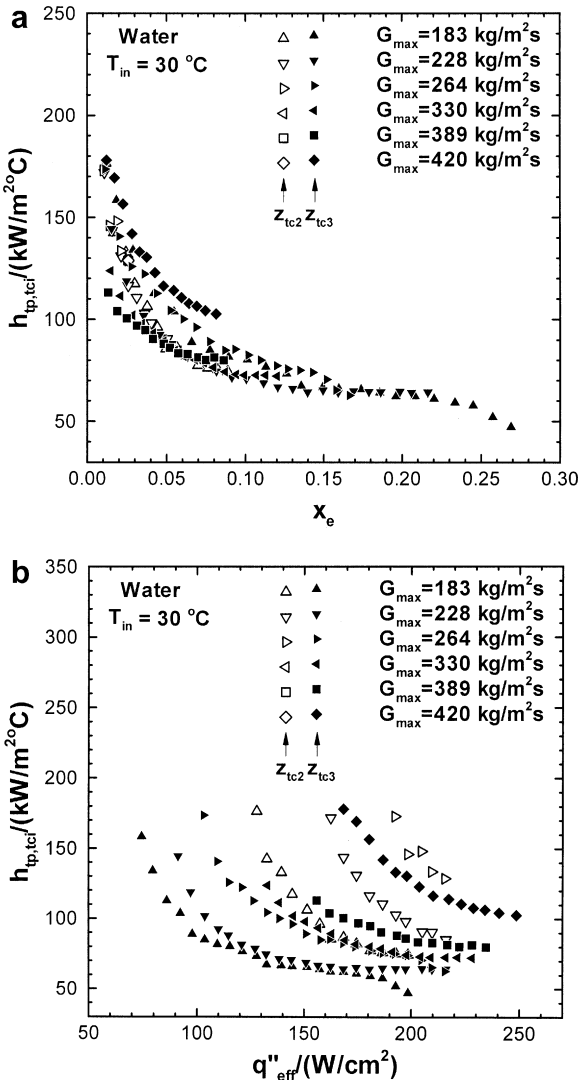

Fig. 8. Variation of measured $h_{tp,tci}$ with (a) $x_{e,tci}$ and (b) q''_{eff} for T_{in} = 30 °C.

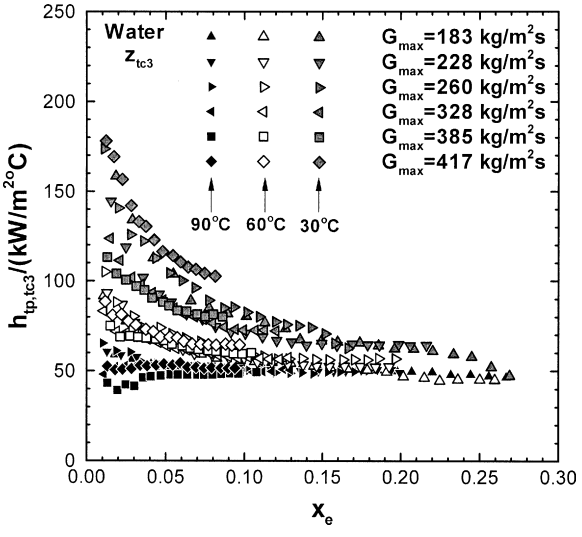

Fig. 9. Variation of measured $h_{tp,tci}$ with $x_{e,tci}$ at z_{tc3} for T_{in} = 90 °C, 60 °C, and 30 °C and all six G_{max}.

In this regime, nucleation is suppressed along the heated surface, and heat is transferred mainly by conduction across the liquid film and evaporation at the liquid–vapor interface. Heat transfer coefficient is dependent upon mass velocity and vapor quality, but less sensitive to heat flux. The general trend is increasing heat transfer coefficient with increasing mass velocity and vapor quality due to reduction in liquid film thickness along the heated surface.

A close examination of the measured variations of $h_{tp,tci}$ with $x_{e,tci}$, G_{max}, and q''_{eff} as shown in Figs. 6–9 reveals that neither nucleate boiling nor two-phase forced convection could be directly applied to explain the observed parametric trends in the present micro-pin-fin array. Figs. 6(b)–8(b) show $h_{tp,tci}$ decreases with increasing q''_{eff} for a constant G_{max}, which is in opposite trend to that associated with nucleate boiling. Figs. 6(a)–8(a) and 9, on the other hand, show $h_{tp,tci}$ is less sensitive to G_{max}, and is either fairly constant (low inlet subcooling) or decreasing (high inlet subcooling) with increasing $x_{e,tci}$, which is not supported by the two-phase forced convection mechanism.

In the present study, two-phase flow patterns in the micro-pin-fin array were examined with the aid of a high-speed video camera. The dominant flow pattern at moderate to high heat fluxes was observed to be annular flow, which is in consistence with the findings from the previous visualization studies [16,17]. In addition, it has been observed that a large number of liquid droplets were entrained in the vapor flow. Based on this observation, two-phase forced convection is believed to be the governing heat transfer mechanism, where heat was first transferred across the liquid film that was formed on the micro-pin-fin surfaces by conduction and then carried away by evaporation at the liquid–vapor interface. Heat transfer behavior, however, was significantly altered by the complex liquid–vapor two-phase transport as a result of the interruptive nature of the flow passages in the micro-pin-fin array. In particular, the large amount of liquid droplets presented in the vapor flow are believed to play a vital role in shaping the unique heat transfer characteristics.

While other mechanisms may exist, it is believed that the liquid droplets in the vapor flow was mostly formed through the following processes: (a) liquid slugs were broken off as discrete droplets at the onset of annular flow, and (b) liquid films were dispersed into the vapor flow as discrete droplets from the downstream edge of the micro-pin-fin side surfaces. While being carried away by vapor flow, a portion of the droplets deposited back onto the front, side, and base surfaces of the micro-pin-fins. It is postulated that the thickness of the liquid film was governed by the following two competing processes: (a) liquid droplet deposition that tended to thicken the liquid film, and (b) vapor flow acceleration and liquid film evaporation that tended to thin the film. It is further postulated that the droplet deposition rate increased with increasing vapor flow velocity in the micro-pin-fin array. In the saturated boiling region, vapor velocity increased with increasing x_e in the flow direction, which led to a rising interfacial shear stress and a decreasing film thickness. On the other hand, the droplet deposition rate would also increase with increasing vapor velocity, which had an opposite effect on the film thickness. It is possible that the net result was a fairly uniform film thickness distribution in the stream-wise direction. It is believed that an increase in G_{max} would not alter the film thickness significantly as both vapor velocity and deposition rate would rise, which again brought in two competing effects on the film thickness.

The above postulated two-phase transport process may explain the observed parametric trends in the micro-pin-fin array. For a near saturated inlet, most liquid droplets in the vapor phase would reach saturated state soon after entering the saturated boiling region. Heat transfer in the saturated boiling region was therefore mainly governed by the film thickness. A uniform film thickness

distribution in the stream-wise direction would lead to a fairly constant heat transfer coefficient, insensitive to both x_e and G_{max}. For a highly subcooled inlet, a substantial amount of liquid droplets might still remain subcooled as they flowed into the low x_e region due to the non-equilibrium effect. These subcooled droplets would enhance heat transfer and yielded higher heat transfer coefficient in the region. Most liquid droplets would eventually reach saturated state in the high x_e region, and the subcooling enhancement effect diminished.

3.3. Assessment of previous heat transfer correlations

Based on the two-phase forced convection mechanism and Reynolds analogy, Krishnamurthy and Peles developed two correlations for water flow boiling heat transfer in an array of circular micro-pin-fins [17]. The two correlations are summarized in Table 2 as correlations 1 and 2. Comparisons between correlation predictions and the present $h_{tp,tci}$ data are shown in Fig. 10(a) and (b). The mean absolute error (*MAE*) for the two correlations, defined as

$$MAE = \frac{1}{M}\frac{|h_{tp,tci,exp} - h_{tp,tci,pred}|}{h_{tp,tci,exp}} \times 100\%, \tag{28}$$

where M is total number of data points, is presented in Fig. 10(a) and (b), respectively. Aside from the scatter in the predicted-to-measured heat transfer coefficient ratio, the two correlations are unable to predict the correct trend of $h_{tp,tci}$ versus $x_{e,tci}$. The deviation may be explained by the fact that the Krishnamurthy and Peles correlation was developed based on the data for circular micro-pin-fins, while the shape of the present micro-pin-fins is square.

3.4. New heat transfer correlation

Deviations in the predictions of previous micro-pin-fin correlations from the present data point to the need for developing a new correlation that can yield more accurate predictions. A new heat transfer correlation is developed based on the following observations: (a) for a near saturated inlet, heat transfer coefficient was fairly constant in the high x_e region, insensitive to both x_e and G_{max}, (b) inlet subcooling enhanced heat transfer in the low x_e region, and (c) the subcooling enhancement effect diminished with increasing x_e. The following functional form is proposed for the present correlation.

$$h_{tp} = Fh_{tp,eq}, \tag{29}$$

where $h_{tp,eq}$ represents the heat transfer coefficient in the high x_e region for a near saturated inlet, and assumes a constant value of 50.44 kW/m^2 °C. $h_{tp,eq}$ is obtained by averaging all $h_{tp,tci}$ data corresponding to T_{in} = 90 °C and $x_{e,tci} \geqslant 0.1$. F in Eq. (29) represents a correction factor accounting for the subcooling enhancement effect. F adopts the following functional form

Table 2
Krishnamurthy and Peles micro-pin-fin correlations [17].

$h_{tp} = \zeta(\phi_l^2)^{0.2475} Pr_f^{0.333} h_{sp}$

$h_{sp} = 0.76\left(\frac{S_L}{d_e}\right)^{0.16}\left(\frac{S_T}{d_e}\right)^{0.2}\left(\frac{H_{fin}}{d_e}\right)^{-0.11}(Re_f)^{0.33}\frac{k_f}{d_e}$

$Pr_f = \frac{c_{pf}\mu_f}{k_f}$

$Re_f = \frac{G_{max}(1-x_e)d_e}{\mu_f}$

Correlation 1:

$\zeta = 1.4, \phi_l^2 = 1 + \frac{0.24}{X_{vv}} + \frac{1}{X_{vv}^2}$

$X_{vv} = \left(\frac{1-x_e}{x_e}\right)^{0.61}\left(\frac{\nu_f}{\nu_g}\right)^{0.5}\left(\frac{\mu_f}{\mu_g}\right)^{0.39}$

Correlation 2:

$\zeta = 1.0, \phi_l^2 = 1 + \frac{0.0385 Re_f}{X_{vv}} + \frac{1}{X_{vv}^2}$

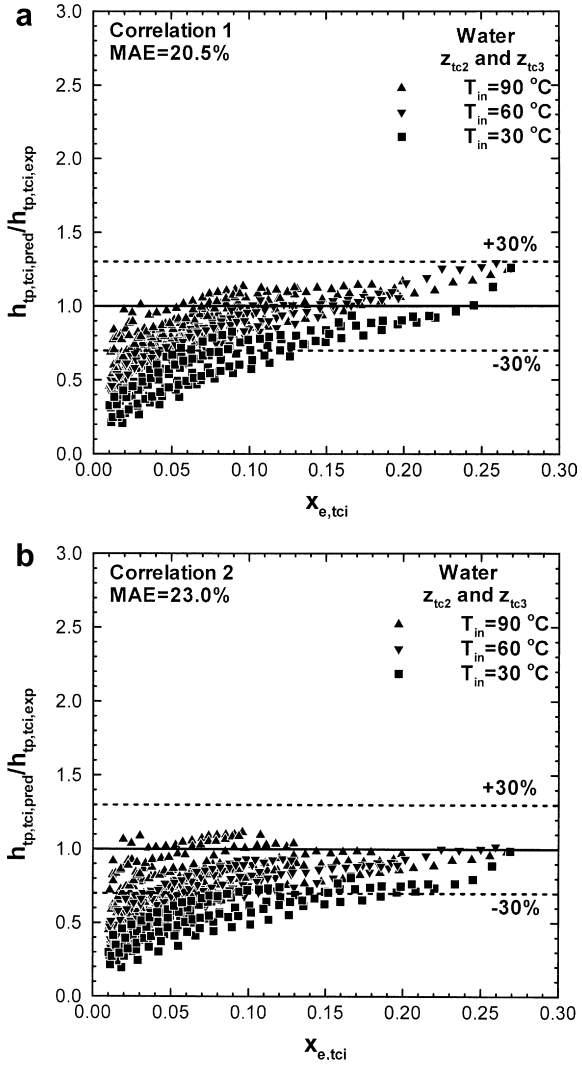

Fig. 10. Comparison of measured $h_{tp,tci}$ with predictions of (a) correlation 1 and (b) correlation 2.

$$F = 1.0 + a_0 x_{e,in} exp[-(a_1 x_{e,in} + a_2)x_e], \tag{30}$$

where $x_{e,in}$ is the thermodynamic equilibrium quality at the micro-pin-fin array inlet. a_0, a_1, and a_2 in Eq. (30) represent empirical constants and are determined to be −12.2, 101, and 29.4 by correlating all $h_{tp,tci}$ data.

Fig. 11(a) compares the predicted and measured $h_{tp,tci}$ versus q''_{eff} for T_{in} = 60 °C and G_{max} = 260 kg/m^2 s. Fig. 11(a) shows the present correlation is able to capture the trend of decreasing $h_{tp,tci}$ with increasing q''_{eff}. The overall predictive capability of the present correlation is shown in Fig. 11(b), which compares the correlation predictions with all $h_{tp,tci}$ data. Nearly all data points are located within a ±30% error band with a mean absolute error (*MAE*) of 7.6%, which demonstrates the excellent predictive capability of the present correlation. It should be noted that the correlation is developed based on the data for water saturated flow boiling ($x_e \geqslant 0.01$) in the micro-pin-fin array under the condition of subcooled inlet ($x_{e,in} < 0$). Experimental validation is needed before the correlation can be applied to conditions beyond which the correlation was originally proposed.

$h_{tp,eq}$ in the present correlation takes a constant value of 50.44 kW/m^2 °C. It is expected that $h_{tp,eq}$ is dependent upon micro-pin-fin geometrical parameters such as W_{fin}, L_{fin}, H_{fin}, S_L, and S_T as the two-phase transport processes are strongly affected by

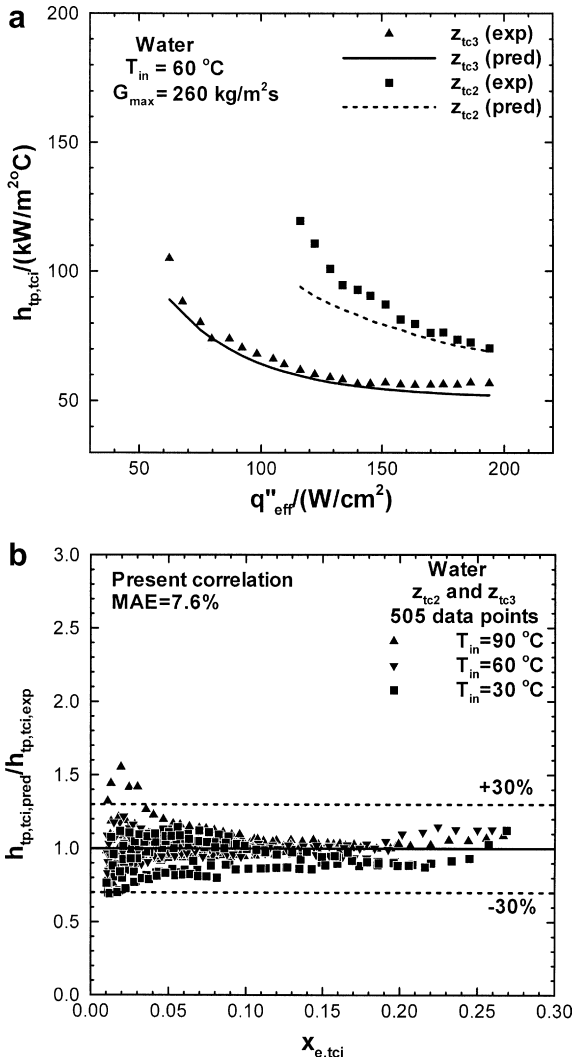

Fig. 11. Comparison of measured $h_{tp,tci}$ with predictions of present correlation: (a) for T_{in} = 60 °C and G_{max} = 260 kg/m^2 s, (b) all $h_{tp,tci}$ data.

the micro-pin-fin geometry. Ideally, $h_{tp,eq}$ should be correlated as a function of these geometric parameters. Unfortunately, such a general correlation for $h_{tp,eq}$ is not possible at present due to the lack of experimental data for water saturated flow boiling heat transfer in staggered square micro-pin-fin arrays having a wide range of geometrical parameters.

4. Conclusions

In this study, experiments were conducted to measure heat transfer coefficient for water saturated flow boiling in an array of staggered square micro-pin-fins. Unique parametric trends were identified and possible heat transfer mechanism was discussed. Previous micro-pin-fin correlations were assessed using the new data. A new heat transfer correlation was developed. Key findings from the study are as follows:

(1) For a near saturated inlet, heat transfer coefficient was fairly constant in the high quality region, insensitive to both quality and mass velocity. Heat transfer in the low quality region was enhanced by inlet subcooling. The enhancement effect due to inlet subcooling diminished with increasing quality.

(2) Two-phase forced convection associated with annular flow was postulated to be the governing heat transfer mechanism. The unique heat transfer characteristics were attributed to the complex liquid–vapor two-phase transport as a result of the interruptive nature of the flow passages in the micro-pin-fin array. In particular, it was believed the liquid droplets entrained in the vapor flow played an important role.

(3) Predictions of two correlations developed by Krishnamurthy and Peles for water saturated flow boiling heat transfer in an array of circular micro-pin-fins were compared to the present data. Significant scatter in data as well as deviation in overall trend point to a need for a new correlation that can yield more accurate predictions.

(4) A new heat transfer correlation was developed based on the unique parametric trends in the micro-pin-fin. Good agreement was achieved between the correlation predictions and the experimental data.

Acknowledgements

The authors are grateful for the support of the National Science Foundation (Award No. CBET07-30315). The micro-pin-fin heat sink test section was fabricated at the Laser-Assisted Multi-scale Manufacturing Laboratory, University of Wisconsin-Madison. Prof. Frank Pfefferkorn and Dr. Yongho Jeon's assistance in fabricating the heat sink test section was greatly appreciated.

References

[1] G.R. Warrier, V.K. Dhir, L.A. Momoda, Heat transfer and pressure drop in narrow rectangular channel, Exp. Thermal Fluid Sci. 26 (2002) 53–64.
[2] W. Qu, I. Mudawar, Flow boiling heat transfer in two-phase micro-channel heat sinks – I. Experimental investigation and assessment of correlation methods, Int. J. Heat Mass Transfer 46 (15) (2003) 2755–2771.
[3] W. Qu, I. Mudawar, Flow boiling heat transfer in two-phase micro-channel heat sinks – II. Annular two-phase flow model, Int. J. Heat Mass Transfer 46 (15) (2003) 2773–2784.
[4] M.E. Steinke, S.G. Kandlikar, An experimental investigation of flow boiling characteristics of water in parallel microchannels, ASME J. Heat Transfer 126 (2004) 518–526.
[5] J.R. Thome, V. Dupont, A.M. Jacobi, Heat transfer model for evaporation in microchannels. Part I: Presentation of the model, Int. J. Heat Mass Transfer 47 (14–16) (2004) 3375–3385.
[6] V. Dupont, J.R. Thome, A.M. Jacobi, Heat transfer model for evaporation in microchannels. Part II: Comparison with the database, Int. J. Heat Mass Transfer 47 (14–16) (2004) 3387–3401.
[7] J. Lee, I. Mudawar, Two-phase flow in high-heat-flux micro-channel heat sink for refrigeration cooling applications: Part II. Heat transfer characteristics, Int. J. Heat Mass Transfer 48 (5) (2005) 941–955.
[8] P.-S. Lee, S.V. Garimella, Saturated flow boiling heat transfer and pressure drop in silicon microchannel arrays, Int. J. Heat Mass Transfer 51 (3–4) (2008) 789–806.
[9] Y. Peles, A. Koşar, C. Mishra, C.J. Kuo, B. Schneider, Forced convective heat transfer across a pin fin micro heat sink, Int. J. Heat Mass Transfer 48 (17) (2005) 3615–3627.
[10] A. Koşar, Y. Peles, Thermal-hydraulic performance of MEMS-based pin fin heat sink, ASME J. Heat Transfer 128 (2) (2006) 121–131.
[11] A. Koşar, Y. Peles, Convective flow of refrigerant (R-123) across a bank of micro pin fins, Int. J. Heat Mass Transfer 49 (17–18) (2006) 3142–3155.
[12] A. Koşar, C. Kuo, Y. Peles, Hydrofoil-based micro pin fin heat sink, in: Proceeding of IMECE 2006, Paper IMECE2006-13257, ASME, 2006.
[13] R.S. Prasher, J. Dirner, J.Y. Chang, A. Myers, D. Chau, D. He, S. Prstic, Nusselt number and friction factor of staggered arrays of low aspect ratio micro-pin-fins under cross flow for water as fluid, ASME J. Heat Transfer 129 (2) (2007) 141–153.
[14] A. Siu-Ho, W. Qu, F. Pfefferkorn, Experimental study of pressure drop and heat transfer in a single-phase micro-pin-fin heat sink, ASME J. Electron. Pack. 129 (4) (2007) 479–487.
[15] W. Qu, A. Siu-Ho, Liquid single-phase flow in an array of micro-pin-fins: Part I. Heat transfer characteristics, ASME J. Heat Transfer 130 (12) (2008) 122402-1–122402-11.
[16] A. Koşar, Y. Peles, Boiling heat transfer in a hydrofoil-based micro pin fin heat sink, Int. J. Heat Mass Transfer 50 (5–6) (2007) 1018–1034.

[17] S. Krishnamurthy, Y. Peles, Flow boiling of water in a circular staggered micro-pin fin heat sink, Int. J. Heat Mass Transfer 51 (5–6) (2008) 1349–1364.
[18] T.H. Hwang, S.C. Yao, Forced convective boiling in horizontal tube bundles, Int. J. Heat Mass Transfer 29 (5) (1986) 785–795.
[19] M.K. Jensen, J.-T. Hsu, A parametric study of boiling heat transfer in a horizontal tube bundle, ASME J. Heat Transfer 110 (4A) (1988) 976–981.
[20] K. Cornwell, The influence of bubbly flow on boiling from a tube in a bundle, Int. J. Heat Mass Transfer 33 (12) (1990) 2579–2584.
[21] S.D. Houston, K. Cornwell, Heat transfer to sliding bubbles on a tube under evaporating and non-evaporating conditions, Int. J. Heat Mass Transfer 39 (1) (1996) 211–214.
[22] R. Dowlati, M. Kawaji, A.M.C. Chan, Two-phase crossflow and boiling heat transfer in horizontal tube bundles, ASME J. Heat Transfer 118 (1) (1996) 124–131.
[23] B.M. Burnside, N.F. Shire, Heat transfer in flow boiling over a bundle of horizontal tubes, Trans. IChemE Part A Chem. Eng. Res. Des. 83 (A5) (2005) 527–538.
[24] W. Qu, A. Siu-Ho, Liquid single-phase flow in an array of micro-pin-fins: Part II. Pressure drop characteristics, ASME J. Heat Transfer 130 (12) (2008) 124501-1–124501-4.
[25] R.D. Blevins, Applied Fluid Dynamics Handbook, Van Nostrand Reinhold Company, New York, 1984.
[26] W. Qu, I. Mudawar, Measurement and prediction of pressure drop in two-phase micro-channel heat sinks, Int. J. Heat Mass Transfer 46 (2003) 2737–2753.
[27] S.J. Kline, F.A. McClintock, Describing uncertainties in single-sample experiments, Mech. Eng. 75 (1) (1953) 3–8.